

Advancements of γ -ray spectroscopy of isotopically identified fission fragments with AGATA and VAMOS++

A. Lemasson^{1,a}, J. Dudouet², M. Rejmund¹, J. Ljungvall³, A. G3rger⁴,
W. Korten⁵

¹GANIL, CEA/DRF-CNRS/IN2P3, Bd Henri Becquerel, BP 55027, F-14076 Caen Cedex 5, France

²Universit3 de Lyon 1, CNRS/IN2P3, UMR5822, IP2I, F-69622 Villeurbanne Cedex, France

³IJCLab, Universit3 Paris-Saclay, CNRS/IN2P3, F-91405 Orsay, France

⁴Department of Physics, University of Oslo, PO Box 1048 Blindern, N-0316 Oslo, Norway

⁵IRFU, CEA, Universit3 Paris-Saclay, 91191, Gif-sur-Yvette, France

the date of receipt and acceptance should be inserted later

Abstract γ -ray spectroscopy of fission fragments is a powerful method for studies of nuclear structure properties. Recent results on the spectroscopy of fission fragments, using the combination of the AGATA γ -ray tracking array and the VAMOS++ large acceptance magnetic spectrometer at GANIL, are reported. A comparison of the performance of the large germanium detector arrays EXOGAM and AGATA illustrates the advances in γ -ray spectroscopy of fission fragments. Selected results are highlighted for prompt γ -ray spectroscopy studies, measurements of short lifetimes of excited states with the Recoil Distance Doppler-Shift method, using both AGATA and VAMOS++ and prompt-delayed γ -ray spectroscopy studies using AGATA, VAMOS++ and EXOGAM.

1 Introduction

Nuclear fission is one of the most effective ways of producing and studying neutron-rich exotic isotopes. Fission fragments cover a wide range of the nuclear chart and exhibit a variety of phenomena ranging from single-particle excitations, near shell closures, to collective excitations related to nuclear vibrations or deformations. The γ -ray spectroscopy of fission fragments can be used to probe the evolution of nuclear structure properties as a function of excitation energy, angular momentum and neutron-proton asymmetry [1–5].

The prompt γ -rays emitted by the secondary fission fragments, as they de-excite to their ground states, provide detailed insight into the structure of nuclei at large spin and isospin. The prompt γ -rays are emitted on a very short time scale (less than few nanosec-

onds), after scission, although sometimes isomers can delay the decay process [6]. The study of prompt γ rays faces the challenge of identifying a particular γ -ray transition among all γ rays emitted by few hundred of fission fragments produced in a single experiment. The use of known characteristic γ rays, in the fragment of interest or in the complementary partner fragment, has been proven to be a powerful tool for characterisation of fission fragments [1, 2]. Experiments making use of high-fold γ -ray coincidence techniques, involving the Gammasphere [7], EUROGAM 2 [8] and EUROBALL [9] arrays, to study fission fragments produced in either spontaneous-fission process or in in-beam heavy-ion induced fission reactions using stable beams, were used to cover a broad range of topics in nuclear structure [1]. More recently, a similar approach was used in conjunction with fission induced by cold and fast neutrons [10, 11].

The necessity of knowledge of the characteristic γ rays could be overcome by employing the isotopic identification techniques of fission fragments using large acceptance magnetic spectrometers such as VAMOS++ [22] and PRISMA [23]. The use of fission induced by reaction in inverse kinematics in conjunction with these large acceptance spectrometers resulted in a higher detection efficiency. This combination has opened new opportunities to study prompt and delayed γ rays emitted by fission fragments [3, 4, 24, 25]. The use of the VAMOS++ spectrometer with the EXOGAM [26] large γ -ray array allowed the first assignment of prompt γ rays in several members of the isotopic chains of Ag [27], Rh [28], Cd and In [24, 25]. The combination of prompt γ -ray data-sets obtained in coincidence with the VAMOS++ magnetic spectrometers with those obtained using high fold γ -ray techniques using Gammasphere

^ae-mail: antoine.lemasson@ganil.fr

Table 1 Summary of the main characteristics of the fission fragment spectroscopy experiments performed with VAMOS++ and AGATA. The beam was ^{238}U at 6.2MeV/A in all the cases.

Exp.	Duration [h]	VAMOS					AGATA			References
		VAMOS- γ [events]	Ang. [deg.]	$B\rho$ [Tm]	Tar./Thick. [μm]	Deg./Thick. [μm]	Dist. [cm]	Crystals	Ang. Range [deg.]	
1	336	4×10^8	20	1.1	$^9\text{Be}/1.6, 5$	-	13.5	32	90-170	[12–15]
2	336	6×10^8	28	1.1	$^9\text{Be}/10$	-	13.3	24	90-170	[16–18]
3	248	2×10^8	28	1.1	$^9\text{Be}/11$	Mg/18.5	18.6	24	120-170	[19, 20]
4	248	4×10^8	19	1.11	$^9\text{Be}/10$	Mg/16.7	23.5	35	120-170	[21]

allowed extended studies in the isotopic chains of Y [29], Pr [30] and Pm [31], which illustrate the complementarity of both methods. Furthermore, the experiments with VAMOS++ and EXOGAM using the Recoil Distance Doppler-Shift Method (RDDS) [32] allowed the measurement of lifetimes of excited states in isotopes of Zr [33], Y and Nb [34] and Tc and Rh [35].

The advent of the new generation of γ -ray tracking arrays AGATA [36] and GRETINA [37] allows an improved determination of the spatial position of the first interaction point of each γ -ray in the detector and an increase of the operating counting rate with larger γ -ray multiplicities. Thus the increased effective granularity results in an improved Doppler correction capability of the energy of the γ -rays emitted by nuclei in flight, provided that the velocity vector \vec{v} of the recoiling fragment is measured on an event-by-event basis with sufficient precision. To ensure that the final Doppler-corrected γ -ray energy resolution only arises from the γ -ray tracking capabilities, resolution in the scattering angle of the fragment better than 1° and resolution in the interaction point at the target than 1 mm, are required.

Furthermore, the continuous angular coverage of γ -ray tracking arrays provides new opportunities for lifetime measurement in the picosecond range based on Doppler-Shift method [38].

This paper presents recent results on the spectroscopy of fission fragments using the AGATA γ -ray tracking array combined with the VAMOS++ large acceptance spectrometer at GANIL [39]. The presented data arise from four experiments (whose main characteristics are described in Table 1) that can be summarised as follows:

- **Exp. 1:** Prompt-delayed γ -ray spectroscopy of $^{122-131}\text{Sb}$ [13], $^{119-121}\text{In}$ [14], $^{130-134}\text{I}$ [15] and experimental methods [12],
- **Exp. 2:** Prompt γ -ray spectroscopy of ^{96}Kr [16] and ^{81}Ga [17], $^{83,85,87}\text{As}$ [18],
- **Exp. 3:** Lifetime measurements in ^{84}Ge , ^{88}Kr , ^{86}Se [19, 20],

- **Exp. 4:** Lifetime measurements in neutron-rich Zr, Mo and Ru [21].

The performance of VAMOS++ for the isotopic identification of fission fragments produced in inverse kinematics is presented in Sec. 2. The Doppler correction of the γ -ray energy is discussed in Sec. 3. A comparison of performances for the spectroscopy of fission fragments between EXOGAM and AGATA is used to illustrate advances in fission fragment spectroscopy. Recent results for prompt γ -ray spectroscopy are highlighted in Sec. 4 and for the measurement of lifetimes of excited states in Sec. 5. Finally, Sec. 6 presents results from prompt-delayed γ -ray spectroscopy with combinations of AGATA and EXOGAM with VAMOS++.

2 Isotopic Identification of Fission Fragments

The fission fragments were typically produced in fusion and transfer induced fission by a ^{238}U beam at the energy of 6.2 MeV/A on a ^9Be target of typical thickness ranging from of 1.6 μm to 10 μm . A typical beam intensity of ~ 1 pA was used. Fission fragments were isotopically identified in terms of atomic number Z , mass number A and atomic charge q , in the VAMOS++ spectrometer, placed at angles between 20 and 28 degrees depending on the fragments of interest. One of the two emitted fragments is detected and isotopically identified in the VAMOS++. The VAMOS++ focal plane detection system consisted of a multi-wire proportional counter (MWPC) (stop of the time-of-flight of the ion), two drift chambers (horizontal and vertical tracking of the fragment trajectory, X, θ, Y, ϕ) and an segmented ionisation chamber (energy loss and energy of the ion, $\Delta E, E$). The ionisation chamber was filled with CF_4 gas at pressures between 70 – 100 mbar, depending on the ions of interest. A dual position sensitive MWPC [40] (DPS-MWPC) (start of the time-of-flight, horizontal and vertical tracking of the fragment trajectory, $\theta_{target}, \phi_{target}$) was placed at the entrance of the spectrometer. The MWPCs and drift chambers were

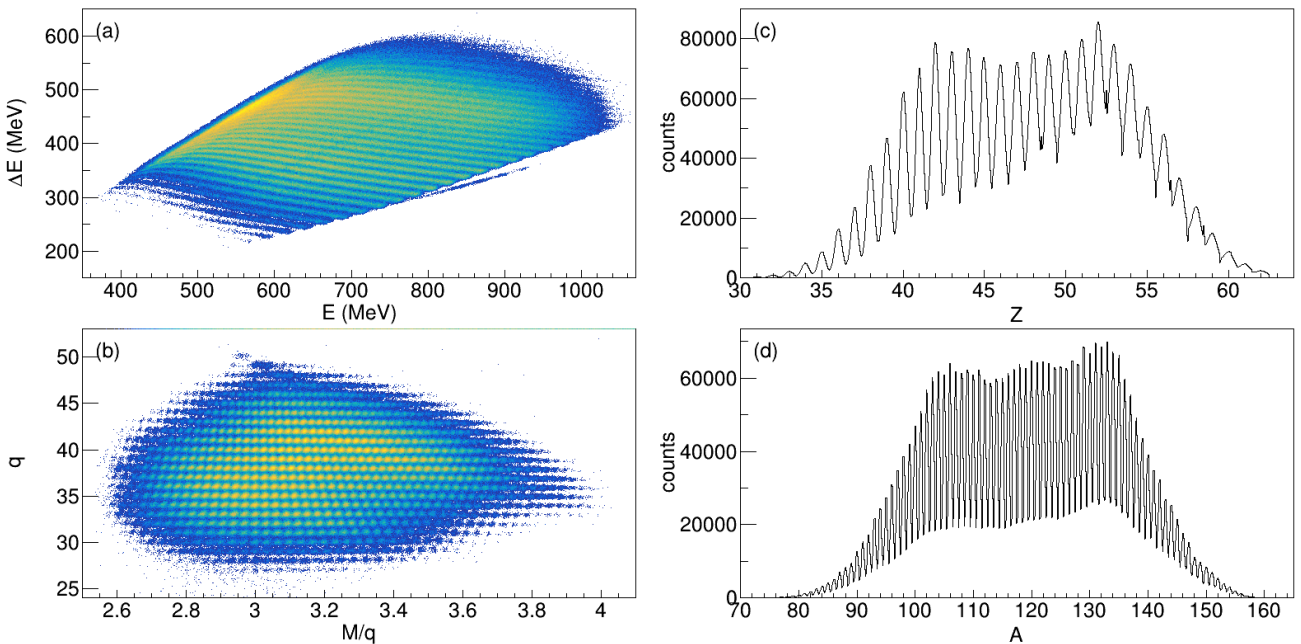


Fig. 1 VAMOS identification spectra for fission fragments produced in the $^{238}\text{U}+^9\text{Be}$ reaction at 6.2 MeV/A (a) two-dimensional spectra of energy loss (ΔE) as function of total energy E measured in ionisation chambers of VAMOS++ (b) two-dimensional spectra of the atomic number Z as a function of the mass-over-charge ratio (M/q) (c) atomic number (Z) distribution (d) atomic mass distribution (A). The data is taken from the Exp. 1, see Table 1.

filled with isobutane gas at a pressure of 6 mbar. The fission fragments were implanted in the gas inside the ionisation chamber. The atomic number Z of the ions was obtained based on $\Delta E - E$ correlation technique. The mass number A was obtained from the reconstructed magnetic rigidity, flight path and the measured time-of-flight. Details on the identification techniques and performances can be found in Ref. [22] while details on the acceptance of the spectrometer for fission reactions are described in Ref. [3]. Typical fission fragment rates in the VAMOS++ focal plane were ranging between 5 and 10kHz and were limited by the pileup in the drift chambers and ionization chambers.

In Fig. 1 the typical identification spectra obtained for fission fragments using VAMOS++ are shown. The two-dimensional correlations are shown in panel (a) energy loss versus total energy (ΔE vs. E) and (b) atomic charge versus mass-over-charge (q vs. M/q). The corresponding one-dimensional spectra are shown in panel (c) atomic number (Z) and (d) atomic mass (A). The data is taken from the Exp. 1, see Table 1.

The velocity vector \vec{v} of the fragment was measured using the DPS-MWPC detector as described in Ref. [40]. Figure 2(a) shows the correlation between the angle of the fragment in the laboratory system (θ_L) detected in VAMOS++ and its velocity v for fission fragments with the atomic number $Z = 40, 50$ and 60 . The data is taken from the Exp. 1, see Table 1. The typical portion of the kinematics of fission fragments measured

can be seen in the figure. The much stronger kinematic focusing of the heavier fragments with respect to the lighter ones can be seen. Figure 2(b) shows the correlation of the angle α , between the γ -ray emission vector \vec{v}_γ versus the velocity vector \vec{v} of the detected fragment (see also Sec. 3), and the velocity v . In Fig. 2 one can observe the angular opening of VAMOS++ (panel (a)) and AGATA (panel (b)). Also, from the range of the velocity v of 2.9 – 4 cm/ns and the mean flight path in VAMOS $D = 760$ cm, one can infer the typical time-of-flight from the target to the focal plane of 190 – 260 ns.

3 Doppler Correction of γ ray energy

The prompt γ rays (γ_P), emitted near the target position were detected by the AGATA [36] γ -ray tracking array and acquired in coincidence with fragment detected in VAMOS. The array was placed at a distances from the target ranging from 13.5 cm to 23.5 cm depending on the configuration used, see Ref. [36, 39] for details of the different configurations. The detection efficiency of the AGATA array in the different configurations is discussed in Refs. [12, 39, 41]. Typical counting rates in the AGATA detectors was ~ 20 kHz per crystal. The AGATA array holding structure and the VAMOS++ spectrometer were supported on a common platform which could rotate around a vertical axis per-

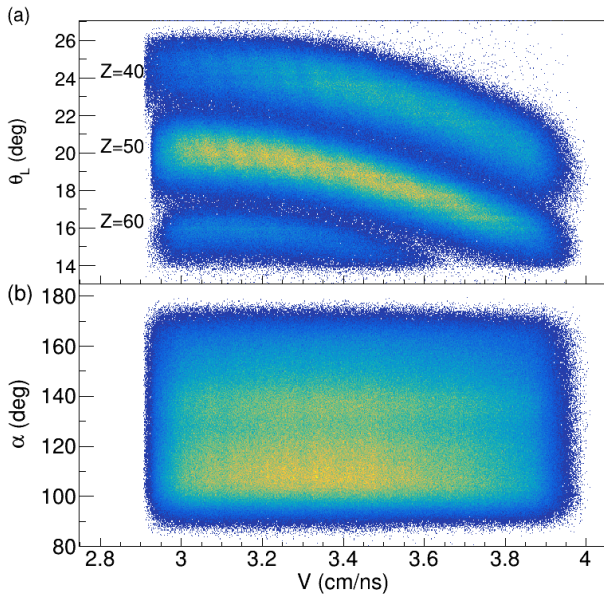


Fig. 2 (a) The laboratory angle θ_L versus the velocity v of fission fragments with the atomic number $Z = 40, 50$ and 60 . (b) The angle α , between the γ -ray emission vector \vec{v}_γ and the velocity vector \vec{v} (see also Sec. 3), versus the velocity v of fission fragments for the same dataset as panel (a). The data is taken from the Exp. 1, see Table 1.

pendicular to the beam axis at the target position. The AGATA detectors typically covered angles from $\sim 100^\circ$ to $\sim 170^\circ$, relative to the axis of the VAMOS++ spectrometer. The γ -ray emission vector \vec{v}_γ was determined using the first three-dimensional interaction point of the γ -ray in the AGATA array, obtained from pulse shape analysis and tracking procedures [36]. A typical position resolution of ~ 5 mm (FWHM) [41–44] has been reported for γ -ray energies around 1.3 MeV. The measured velocity vector of the detected fragment \vec{v} and γ -ray emission vector \vec{v}_γ were used to derive the Doppler-corrected γ -ray energy on an event-by-event basis. The Doppler correction was obtained using the following relationship

$$E_{RF} = E_{LAB} \cdot (1 - \beta \cdot \cos(\alpha)) \cdot \gamma$$

where: E_{RF} and E_{LAB} are respectively the energies of the γ ray in the rest frame of the nucleus and in the laboratory system, $\beta = v/c$, $\gamma = \frac{1}{\sqrt{1-\beta^2}}$ and α is the angle between vector \vec{v} and \vec{v}_γ . It should be noted that γ rays emitted by the complementary fragment will have an incorrect doppler correction applied, resulting in Doppler broadened and shifted peaks that contribute to the background of the spectra. It was demonstrated in Refs. [3, 4] that Doppler correction for the binary partner can be achieved using two-body kinematics derived from the velocity vector of the measured fragment.

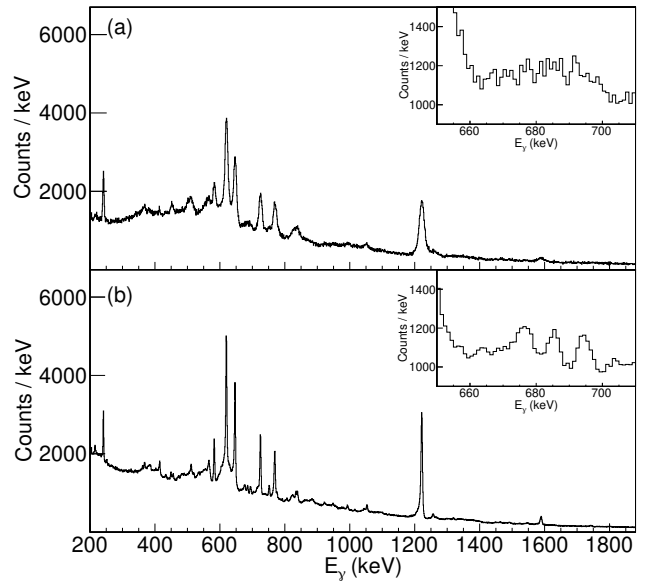


Fig. 3 Prompt Doppler-corrected γ -ray spectra measured in coincidence with isotopically identified ^{98}Zr in VAMOS++: (a) with γ rays measured with the EXOGAM array (b) with γ rays measured with AGATA γ -ray tracking array. The two γ -ray spectra are normalised to the same total number of counts. The insets highlight part of the corresponding γ -ray spectra in the 650 keV to 710 keV range.

4 Prompt- γ -ray spectroscopy

4.1 AGATA versus EXOGAM

To illustrate the performances obtained with AGATA for the prompt- γ -ray spectroscopy of fission fragments, the Fig. 3 shows Doppler-corrected γ -ray spectra in coincidence with isotopically identified ^{98}Zr in VAMOS++. Figure 3(a) shows the prompt γ rays measured with the EXOGAM array [26] consisting of 11 Compton-suppressed segmented clover HPGe detectors (15 cm away from the target), in coincidence with the isotopically identified fragments. The \vec{v} of the fragment along with the position of the center of the electrical segment of the clover detector that had registered the highest energy deposit were used to obtain the γ -ray energy in the rest frame of the emitting fragment [45]. Figure 3(b) shows the prompt γ rays measured with the AGATA array in coincidence with the isotopically identified fragments. The data is taken from Exp. 1, see Table 1.

The comparison of the spectra clearly illustrates the improved γ -ray energy resolution arising from the position resolution of the first interaction point derived in AGATA. The 1222.9 keV γ ray, $2^+ \rightarrow 0^+$ transition in ^{98}Zr , can be used to evaluate the obtained energy resolution of Doppler-corrected spectra. Considering all

clovers from EXOGAM (including 90° and 135° rings), a resolution of 15 keV was obtained. Considering only backward angles in EXOGAM, a resolution of 7 keV was measured. This is to be compared with a resolution of 5 keV obtained with AGATA for angular coverage ranging from 100° to 170° . The improved resolving power can be further seen in the insets of Fig. 3, where within an expanded region of the γ -ray spectra several weak transitions, unresolved using the EXOGAM array, could be resolved using the AGATA array.

4.2 γ -ray spectroscopy of ^{96}Kr

The sudden appearance of the onset of the collectivity at $N = 60$ has been one of the early successes of the γ -ray spectroscopy of fission fragments. After decades of studies establishing the sudden transition towards the deformation at $N = 60$ in Zr ($Z = 40$) and Sr ($Z = 38$), the detailed description of this island of deformation still challenges theoretical models. In Ref. [16], the prompt γ -ray spectroscopy of the neutron-rich ^{96}Kr ($Z = 38$ and $N = 60$) has contributed to delineate the limits of this island of deformation. The nucleus of interest, ^{96}Kr , was produced in transfer- and fusion-induced fission processes, using the ^{238}U beam impinging on a ^9Be target. This experiment is referred to as Exp. 2, see Table 1. The prompt Doppler-corrected γ -ray spectrum measured in coincidence with ^{96}Kr isotopically identified in VAMOS++ is shown in Fig 4(a). Three γ -ray transitions at the energies of 554(1) keV, 621(2) keV, and 515(2) keV can be seen in the spectrum. The 554 keV transition confirms the excitation energy of the first 2^+ state of Ref. [46]. The 621 keV transition was observed in coincidence with the 554 keV transition as can be seen in the inset in Fig.4(a). It was interpreted as the transition depopulating the first 4^+ excited state at the energy of 1175(3) keV. Because of the limited statistics, it was not possible to obtain a significant coincidence analysis for the 515 keV transition which was not placed in the level scheme. The presence of low-lying 2^+ excited states in the Kr isotopic chain suggests the possible assignment of the 515 keV γ ray to the $2^+_2 \rightarrow 2^+_1$ transition.

Recently, the spectroscopy of ^{96}Kr from knock-out and inelastic reactions was reported [49]. A $888(16)$ keV state, decaying by 887^{+24}_{-23} keV and $334(16)$ keV γ -ray transitions, was tentatively assigned to the 2^+_2 state based on coincidence arguments. These γ -ray transitions were not observed in Ref. [16] due to the available statistics. The 515 (2) keV transition was also observed and reported in coincidence with the $2^+ \rightarrow 0^+$ transition, but it was not placed either in the level scheme.

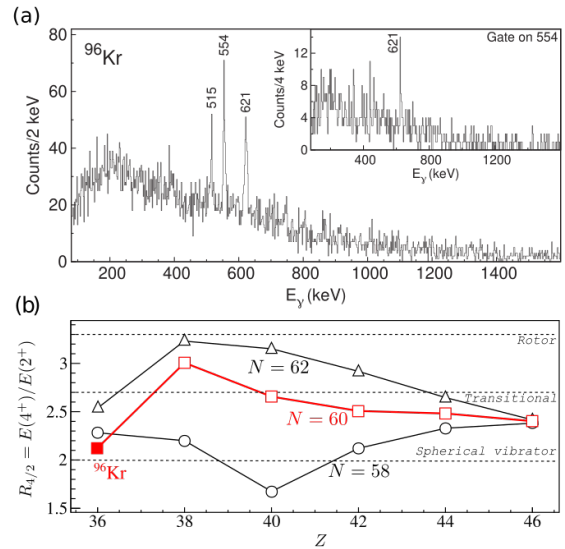


Fig. 4 The data is obtained from the Exp. 2, see Table 1. (a) Doppler-corrected γ -ray spectra measured in AGATA in coincidence with ^{96}Kr detected and identified isotopically in VAMOS++ [16]. (Inset) γ -ray spectrum measured in coincidence with the 554 keV transition. (b) The $R_{4/2}$ ratio against the atomic number Z for $N = 58$ – 62 isotonic chains. Horizontal dashed lines represent a schematic classification between spherical vibrational and rotor nuclei from Ref. [47]. The $R_{4/2}$ point for ^{98}Kr at $N = 62$ obtained from Ref. [48] has been added to the figure. The figure is adapted from Ref. [16] CC BY 4.0. © 2017, J. Dudouet *et al.*, published by American Physical Society.

The nature of the state depopulated by the 515 keV transition remains an open question to be addressed.

To understand, quantify, and characterise the evolution of the nuclear structure along isotopic chains, a systematic study of the energy ratio $R_{4/2} = E(4^+)/E(2^+)$ is often used [47]. The newly measured energy of the 4^+ state results in the energy ratio of $R_{4/2} = 2.12(1)$. In Fig.4(b) the $R_{4/2}$ ratio is shown as a function of atomic number Z for isotonic chains with $N = 58, 60$ and 62 . It is seen that at the $N = 58$ the nuclei between Kr and Pd exhibit very little collectivity and are situated between the transitional and spherical vibrator regime. For $N = 60$ and 62 , the collectivity increases with decreasing Z , reaching the maximum in Sr. In ^{96}Kr one observes an abrupt decrease of the collectivity. The $R_{4/2}$ obtained for ^{98}Kr [48] follows the same behaviour. This new measurement highlights an abrupt transition of the degree of collectivity as a function of the proton number at $Z = 36$. A possible reason for this abrupt transition could be related to the insufficiently large amplitude of the proton excitation in the $g_{9/2}$, $d_{5/2}$, and $s_{1/2}$ orbitals to generate strong quadrupole correlations or coexistence of competing different shapes.

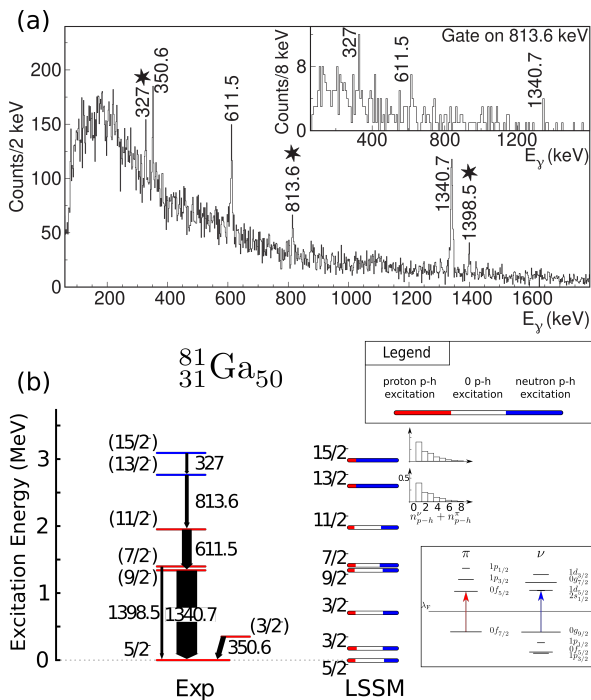


Fig. 5 (a) Tracked Doppler-corrected γ -ray spectrum measured in coincidence with the isotopically identified ^{81}Ga . Known transitions are labelled by their energy, while newly reported transitions are marked with an additional star symbol. The inset shows the γ - γ coincidence spectrum gated on the 813.6 keV transition in ^{81}Ga . (b) Experimental and theoretical level schemes of ^{81}Ga . The experimental levels marked with red (blue) correspond to dominant contribution from $0p-h$ ($1p-h$) excitations of the ^{78}Ni core. The data is obtained from the Exp. 2, see Table 1. The figure is adapted with permission from Ref. [17], © 2019, by American Physical Society.

This measurement established the Kr isotopic chain as the low- Z boundary of the island of deformation for $N = 60$ isotones. The comparison with available theoretical predictions using different beyond mean-field approaches shows that these models fail to reproduce the abrupt transitions at $N = 60$ and $Z = 36$ and that the precise description of the region remains challenging. See Ref. [16] for further details.

4.3 γ -ray spectroscopy of ^{81}Ga

It is agreed that ^{78}Ni ($Z = 28$, $A = 50$) manifests a doubly magic character. However, in Ref. [50] the sudden emergence of collective states and their coexistence with the spherical states are predicted. These spherical states arise mainly from one particle-hole excitations across the magic shell gaps ($Z = 28$ and $N = 50$). Collective states arise from multi particle-hole excitations, giving rise to a deformed collective band, provid-

ing a striking example of shape coexistence. The excited states of $N = 50$ isotones provide complementary insight into the coupling of single particle-hole configurations with valence protons where the particle-hole configuration are intimately related to the properties of the $N = 50$ shell gap.

The high-spin states of the neutron-rich ^{81}Ga , with three valence protons outside a ^{78}Ni core, were measured for the first time [17]. This experiment is referred to as the Exp. 2, see Table 1. The tracked Doppler-corrected γ -ray spectrum obtained in coincidence with ^{81}Ga is shown in Fig. 5(a). The inset shows the γ - γ coincidence spectrum gated on the 813.6 keV transition. The derived level scheme is shown in Fig. 5(b). The newly observed high-spin states in ^{81}Ga are interpreted using the results of state of the art Large Scale Shell Model (LSSM) calculations [50] using the PFSDG-U interaction, see Fig. 5(b). The lower excitation energy levels are understood as resulting from the recoupling of three valence protons to the closed doubly magic core, while the highest excitation energy levels correspond to excitations of the magic $N = 50$ neutron core.

These results support the doubly magic character of ^{78}Ni and the persistence of the $N = 50$ shell closure, but also highlight the presence of strong proton-neutron correlations associated with the promotion of neutrons across the magic $N = 50$ shell gap, only few nucleons away from ^{78}Ni . See Ref. [17] for further details.

5 Lifetime measurement using RDDS method

5.1 RDDS method

The Recoil Distance Doppler-Shift method is a well-established technique for the determination of picosecond lifetimes of excited nuclear states. Traditionally, a nucleus produced in a nuclear reaction in a thin target leaves the target with a velocity v_t and is stopped after flying through a well-defined distance in a stopper foil. The excited state in the nucleus can de-excite by an emission of a γ ray either in-flight or at rest in the stopper foil. One can observe, the intensity of either Doppler-shifted (S) or unshifted (U) components of the γ -ray transition, respectively. The lifetime of the corresponding state can be measured using the so called decay curve or flight curve based on the intensities of the Doppler-shifted and unshifted components. An alternative procedure called the Differential Decay Curve Method (DDCM) is also used. See further details in Ref. [32].

For the experiments, where the recoiling nuclei of interest are to be detected, as it is the case when using VAMOS++ spectrometer, the stopper foil can be

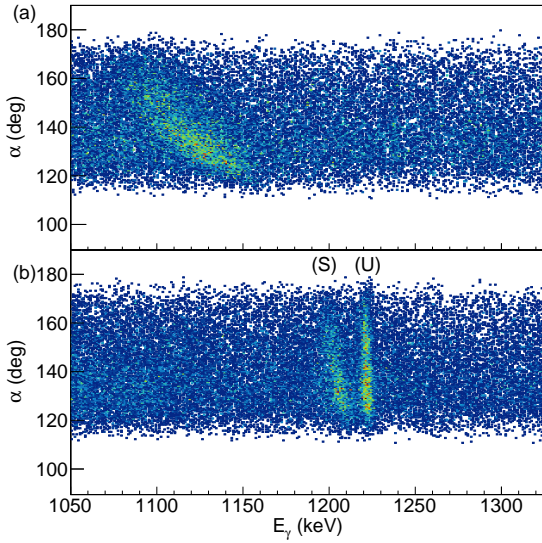


Fig. 6 Two dimensional spectra of the angle α (the angle between vector \vec{v}_d^+ and \vec{v}_γ^+) as a function of the γ -ray energy for a target-to-degrader distance of $470 \mu\text{m}$ in coincidence with ^{98}Zr identified in VAMOS++, (a) detected in the laboratory frame (b) Doppler-corrected using the fragment velocity after the degrader \vec{v}_d^+ . The unshifted (U) and Doppler-shifted (S) components are marked. The data is taken from the Exp. 4, see Table 1.

replaced by a degrader foil. One can observe either the γ rays emitted after the target at the recoil velocity v_t or after the degrader foil at v_d . Typically, the Doppler correction uses the velocity of the nucleus measured after the degrader v_d , therefore the γ rays emitted after the degrader are seen as unshifted and those emitted before the degrader as Doppler-shifted.

In Fig. 6(a), the γ -ray energy measured in the laboratory frame is shown as function of the angle α , between the vectors \vec{v}_d^+ and \vec{v}_γ^+ , in coincidence with isotopically identified ^{98}Zr in VAMOS++ for the target-to-degrader distance of $470 \mu\text{m}$ in the Exp. 4, see Table 1. In Fig. 6(b) the same events are shown, but a Doppler correction on an event-by-event basis was applied using the measured velocity vector after the degrader \vec{v}_d^+ . The well-defined in energy, unshifted (U) component can be seen in the figure. The Doppler-shifted (S) component becomes dependent on α and appears at a lower energy because the γ ray was emitted at a larger velocity, $v_t > v_d$, and the AGATA array was placed at backward angles, $\alpha > 90^\circ$.

The use of the AGATA array for lifetime measurements using the RDDS method has several important assets namely (i) a very good energy resolution for Doppler-corrected γ -ray transitions, (ii) a good coverage for the very backward solid angle where the Doppler effect is largest (iii) the availability of a continuous measurement of the angle α , see Fig. 6.

5.2 AGATA versus EXOGAM

Doppler-corrected γ -ray spectra of several transitions in ^{98}Zr , isotopically identified in VAMOS++, are shown in Fig. 7. Panels (a) and (b) show spectra obtained with AGATA [21] from Exp. 4, see Table 1. Panels (c) and (d) show corresponding spectra with comparable target-to-degrader distances obtained with EXOGAM [33]. Panels (a) and (c) show the components of the 1223 keV transition de-exciting the 2^+ state ($\tau = 3.8 \pm 0.8$ ps) and panels (b) and (d) the 620 keV and 647 keV transitions de-exciting the 4^+ ($\tau = 7.5 \pm 1.5$ ps) and 6^+ ($\tau = 2.6 \pm 0.9$ ps) states. The evolution of the intensity of the Doppler-shifted (S) component relative to the unshifted (U) component, for the transitions de-exciting the states with different lifetimes, is evident as a function of the target-to-degrader distance. The improved energy separation between the two components, due to the improved first interaction position of the γ ray and thus its energy resolution can be also seen in the figure. This results in an improved the precision of the lifetime analysis and extracted reduced transition strength.

5.3 Lifetime measurement of excited states in ^{84}Ge

The recent intense experimental and theoretical efforts on the investigation of the nuclear structure in the vicinity of doubly magic ^{78}Ni ($Z = 28$, $N = 50$), have triggered experimental measurements of lifetimes of excited states.

In Ref. [19], lifetime measurements of excited states of the light $N = 52$ isotones ^{88}Kr ($Z = 36$), ^{86}Se ($Z = 34$), and ^{84}Ge ($Z = 32$) using the RDDS method with VAMOS++ and AGATA were reported. The reduced electric quadrupole transition probabilities $B(E2, 2^+ \rightarrow 0^+)$ and $B(E2, 4^+ \rightarrow 2^+)$ were obtained for the first time for the hard-to-reach ^{84}Ge . The nuclei of interest were produced in transfer- and fusion-induced fission processes, using the ^{238}U beam impinging on a ^9Be target followed by a Mg degrader. This experiment is referred to as the Exp. 3, see Table 1.

Because of low statistics, the RDDS-analysis variant developed in Ref. [54] had to be applied, which consists in summing the statistics obtained over all distances and determining the lifetime, see Ref. [19] for further details.

The obtained $B(E2)$ values are placed in the systematics of light $N = 52$ isotones in Fig. 8, where a comparison with several calculations is also provided.

Shell-model results from Ref. [53] (open circles), assuming an inert ^{78}Ni core, are in excellent agreement with the experimental values (closed circles) obtained

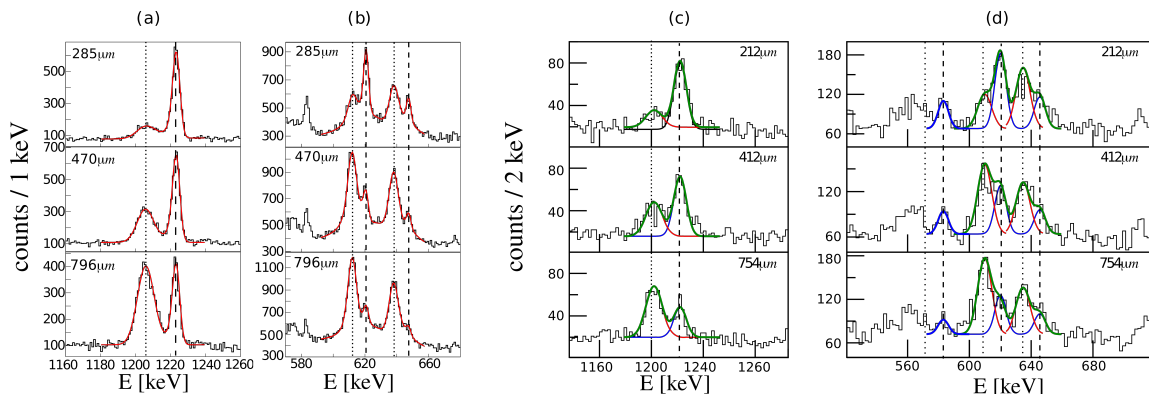


Fig. 7 Comparison of Doppler-corrected γ -ray spectra using \vec{v}_d , measured in coincidence with isotopically identified ^{98}Zr in VAMOS++ obtained with AGATA (a) and (b) and EXOGAM (c) and (d). The target-to-degrader distances are given. Panels (a) and (c) show Doppler-shifted and unshifted components for the 1222.9 keV transition de-exciting the 2^+ state. Panels (b) and (d) show Doppler-shifted and unshifted components of the 620.5 keV and 647.6 keV transitions de-exciting the 4^+ and 6^+ states. The data from the AGATA array is taken from the Exp. 4, see Table 1 and adapted from Ref. [21]. The panel (c) and (d) for the EXOGAM array are adapted with permission from Ref. [33], © 2018, by American Physical Society.

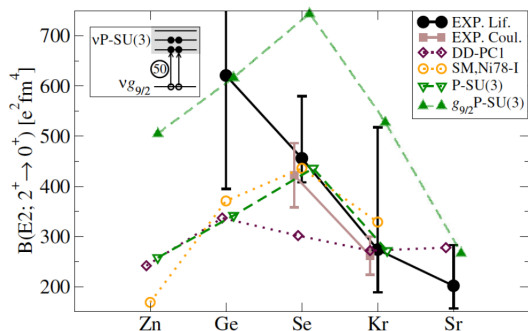


Fig. 8 $B(E2; 2^+ \rightarrow 0^+)$ systematic of the light $N = 52$ even-even isotones from $Z = 38$ down to $Z = 30$. "Exp. Lif.": experimental values from lifetimes measurements (from Ref. [19], except Sr [51]); "Exp. Coul.": experimental values from Coulomb excitation measurements [52]; "DD-PC1": beyond mean-field calculations using the relativistic functional DD-PC1 (Ref. [19]); "SM,Ni78-I" shell-model calculations from [53]; "($g_{9/2}$) P-SU(3)": pseudo-SU(3) limit [53] (or including one $N = 50$ core-breaking $g_{9/2}$ pair promotion, as illustrated by the inset). The data is obtained from the Exp. 3, see Table 1. (The figures are adapted from Ref. [19] CC BY 4.0. © 2018, C. Delafosse *et al.*, published by American Physical Society).

for ^{88}Kr and ^{86}Se . Interestingly enough, both shell-model and experimental values exhaust the limit for pure pseudo-SU(3) symmetry (down triangles) for these two isotones. This clearly means that the quadrupole coherence offered by this subspace is maximally expressed in these two nuclei. In contrast, both shell-model and pseudo-SU(3) values barely reach the lower tip of the experimental error bar for ^{84}Ge . The more in-depth analysis of the experimental data in Ref. [19] suggests, for the first time, a shape transition from $Z = 34$ (soft triaxial) to $Z = 32$ (prolate deformed), a result all

the more unexpected as the shell model predicts a "fifth island of inversion" only for much lighter ($Z < 28$) systems [50].

6 Prompt-delayed γ -ray spectroscopy

6.1 Experimental method

A new experimental setup to measure prompt-delayed γ -ray coincidences from isotopically identified fission fragments, over a wide time range, 100 ns - 200 μs , is presented in Ref. [12]. The fission fragments are isotopically identified, on an event-by-event basis, using the VAMOS++ large acceptance spectrometer. The prompt γ rays (γ_P) emitted near the target were detected using the AGATA γ -ray tracking array. The fission fragments reaching the focal plane after a typical time-of-flight of ~ 200 ns, were stopped in the ionisation chamber. Delayed γ rays (γ_D) were detected using seven EXOGAM HPGGe Clover detectors [26] arranged in a wall-like configuration at the focal plane of the VAMOS++ spectrometer. A 2 mm thick aluminium window between the ionisation chamber and the Clover detectors was used to minimise the attenuation of the emitted γ rays. A 3 mm thick lead shielding was placed after and in-between the Clover detectors to minimise the events arising from the room-background and Compton scattering between the Clover detectors. The details of the experimental setup and analysis methods are discussed in Ref. [12].

The results obtained using this experimental setup will be illustrated based on the case of well studied ^{132}Te [55–62]. Figure 9(a) shows the partial level scheme of ^{132}Te (below 4.3 MeV). Several different isomeric

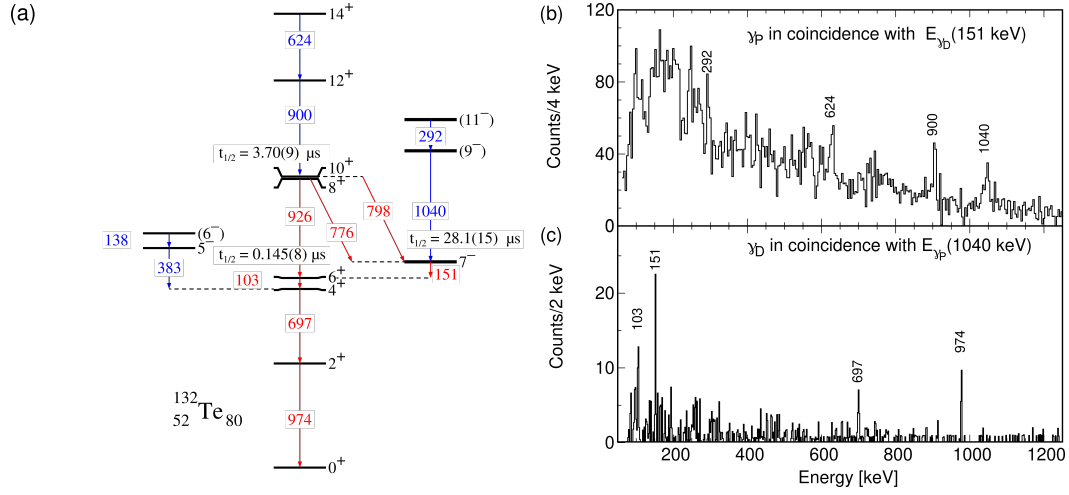


Fig. 9 (a) The partial level scheme of ^{132}Te (below 4.3 MeV). The transitions above (below) isomeric states are indicated in blue (red). (b) ^{132}Te Doppler-corrected prompt γ ray (γ_P) spectrum with the condition that a delayed γ ray with energy $E_{\gamma_D} = 151$ keV was detected. (c) ^{132}Te delayed γ ray (γ_D) spectrum in coincidence with the prompt $E_{\gamma_P} = 1040$ keV γ ray. The data is taken from the Exp. 1, see Table 1. The figures reproduced with permission from Ref. [12], © 2017, published by Springer.

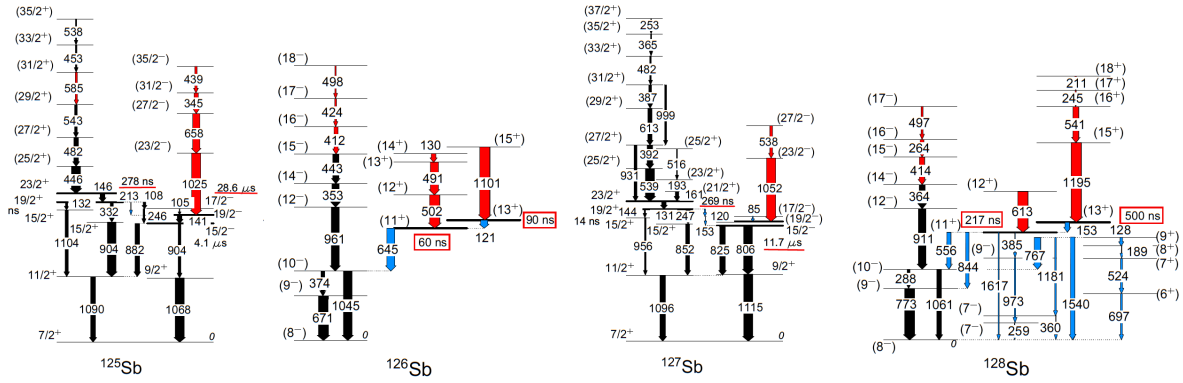


Fig. 10 The level schemes of $^{125}\text{--}^{128}\text{Sb}$. The newly observed γ -ray transitions above and below the isomer are indicated in red and blue, respectively. The width of the arrows represent the intensity of the transitions. The isomeric states are indicated by a thick line. Previously known half-lives that were remeasured in Ref. [13] have been underlined by a red line, whereas the newly measured half-lives have been marked with a red box. The half-lives not measured in Ref. [13] are also shown. The data is taken from the Exp. 1, see Table 1. The figure is adapted from Ref. [13] CC BY 4.0. © 2017, S. Biswas *et al.*, published by American Physical Society.

states have been reported for this nucleus, in particular, the 7^- excited state at 1925 keV with the half-life of $t_{1/2} = 28.1 \mu\text{s}$ [58]. In earlier works the prompt transitions 1040 keV and 292 keV have been observed and placed tentatively in the level scheme as feeding the 7^- state [59, 62]. However, the prompt-delayed correlation between the γ rays populating and depopulating the 7^- state could not be observed. In Fig. 9(b) the Doppler corrected prompt γ ray (γ_P) spectrum observed in coincidence with delayed $E_{\gamma_D} = 151$ keV γ -ray, which depopulates the 7^- isomeric state, is shown. The prompt γ rays 292 keV, 624 keV, 900 keV and 1040 keV, are seen in the spectrum. Figure 9(c) shows the delayed γ -ray spectrum in coincidence with the prompt $E_{\gamma_P} = 1040$ keV. The delayed γ rays 103 keV, 151 keV, 697 keV

and 974 keV, are seen in the spectrum. This measurement confirms experimentally proposed the level scheme, and illustrates the capabilities of the VAMOS-AGATA-EXOGAM setup to properly correlate prompt and delayed γ rays across a long-lived isomer. Further details are discussed in Ref. [12].

6.2 Prompt-delayed γ -ray spectroscopy of neutron-rich isotopes of Sb

The $Z = 50$ shell closure, near $N = 82$, is unique in the sense that it is the only shell closure with the spin-orbit partner high-spin orbitals, $\pi g_{9/2}$ and $\pi g_{7/2}$, enclosing the magic gap. The interaction of the pro-

ton hole/particle in the above-mentioned orbitals with neutrons in the high-spin $\nu h_{11/2}$ orbital is an important prerequisite to the understanding of the nuclear structure near $N = 82$ and establishing the features of the $\nu\pi$ interaction.

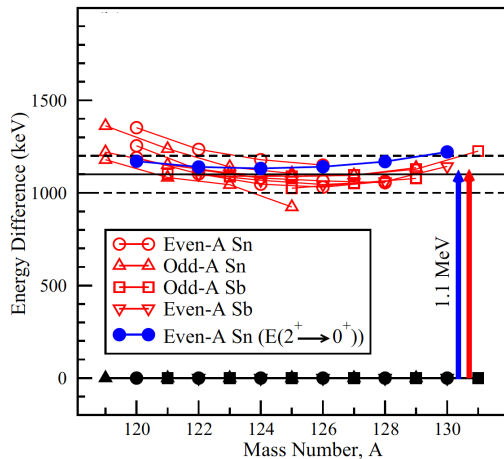


Fig. 11 Plot of the energy differences between states with neutron seniority $\nu_\nu = n$ and $\nu_\nu = n + 2$ ($n = 0, \dots, 4$), for odd- A and even- A $^{119-130}\text{Sn}$ and $^{121-131}\text{Sb}$ nuclei. Figure reproduced from [13] CC BY 4.0. © 2017, S. Biswas *et al.*, published by American Physical Society

Prompt-delayed γ ray of high-spin states in neutron-rich $^{122-131}\text{Sb}$ ($Z = 51$) [13], $^{130-134}\text{I}$ ($Z = 53$) [15] and $^{119,121}\text{In}$ ($Z = 49$) [14], using the unique experimental setup combining AGATA, VAMOS++ and EXOGAM were reported. This experiment is referred to as the Exp. 1, see Table 1. In this section we will restrict ourselves to the isotopes of Sb [13].

Figure 10 shows the level schemes of $^{125-128}\text{Sb}$. The newly observed γ -ray transitions above and below the isomer are indicated in red and blue, respectively. Previously known half-lives have been remeasured and are underlined by a red line, whereas the newly measured half-lives are marked with a red box. The wealth of the new experimental data obtained in Ref. [13] can be clearly seen from the figure.

The experimental data was compared with theoretical results obtained from LSSM. A consistent agreement with the excitation energies and the $B(E2)$ transition probabilities in neutron-rich Sn and Sb isotopes was obtained. The isomeric configurations in Sn and Sb were found to be relatively pure. The LSSM calculations revealed that the presence of a single valence proton, mainly in the $\pi g_{7/2}$ orbital in Sb isotopes, leads to significant mixing, due to the $\nu\pi$ interaction, of (i) the neutron seniorities (ν_ν)¹ and (ii) the neutron an-

¹ ν_ν stands for neutron seniority, which refers to the number of unpaired neutrons

gular momentum (I_ν). The above features have a weak impact on the excitation energies, but have an important impact on the nuclear wave function of the excited states and thus on the corresponding $B(E2)$ transition probabilities. In addition, a striking feature of the constancy of the energy differences, where the increase in the number of broken neutron pairs is involved, was observed. A plot of such energy differences in $^{119-130}\text{Sn}$ and $^{122-131}\text{Sb}$ isotopes is shown in Fig. 11. This figure shows that the average energy for the breaking of the first and second pair of neutrons is ~ 1.1 MeV, and that this energy is constant (with a deviation of ~ 100 keV) for a wide range of mass numbers, irrespective of the excitation energy and mixing of neutron seniorities (ν_ν) in the case of Sn and Sb. In addition, it follows the behavior of even- A Sn isotopes for $E(2^+ \rightarrow 0^+)$. Further details are discussed in Ref. [13].

7 Summary and Conclusions

Among a large variety of experiments performed at GANIL using the AGATA γ -ray array, four have focussed on the nuclear structure studies of isotopically identified fission fragments employing the VAMOS++ magnetic spectrometer in coincidence.

The combination of the AGATA γ -ray array with the VAMOS++ spectrometer forms a unique, highly performant experimental setup combining efficiency with counting rate capabilities, as well as selectivity with excellent Doppler correction of γ -ray energy and precise isotopic identification. The performed experiments have been very fruitful and numerous pertinent results have been obtained including the γ -ray spectroscopy of ^{96}Kr [16], ^{81}Ga [17], $^{83,85,87}\text{As}$ [18], lifetime measurements of excited states using the RDDS method in ^{84}Ge , ^{88}Kr , ^{86}Se [19, 20], neutron-rich Zr, Mo and Ru [21] and prompt-delayed γ -ray spectroscopy, using the EXOGAM array for delayed γ rays, of $^{122-131}\text{Sb}$ [13], $^{119-121}\text{In}$ [14] and $^{130-134}\text{I}$ [15].

In the future, fission fragments spectroscopy program will be pursued at LNL using combination of AGATA and the PRISMA [23] spectrometer. The ongoing development of ^{238}U beams at energies around the Coulomb barrier will extend measurements using inverse kinematics reactions in addition to presently available ^{208}Pb beams. Further, the increased number of available AGATA crystals will allow to cover 2π solid angle at the nominal detector distance, effectively doubling the solid angle coverage compared to the experiments presented in this work. This will improve the $\gamma-\gamma$ coincidence efficiency, allowing to expand investigations of exotic neutron-rich nuclei by fission-fragment spectroscopy.

Acknowledgments

The authors thank the AGATA collaboration, the e661, e680, e669 and e706 GANIL experimental collaborations and the technical teams at Grand Accélérateur National d'Ions Lourds for their support during the experiments. A.G. has received funding from the Norwegian Research Council, project 325714.

References

1. J. Hamilton, *et al.*, *Prog. Part. Nucl. Phys.* **35**, 635 (1995).
2. I. Ahmad and W. R. Phillips, *Rep. Prog. Phys.* **58**, 1415 (1995).
3. A. Navin, *et al.*, *Phys. Lett. B* **728**, 136 (2014).
4. A. Navin and M. Rejmund, in *McGRAW-HILL Yearbook of Science and Technology* (2014) p. 137.
5. S. Leoni, C. Michelagnoli, and J. N. Wilson, *La Rivista del Nuovo Cimento* **45**, 461 (2022).
6. V. Metag, D. Habs, and H. Specht, *Physics Reports* **65**, 1 (1980).
7. I. Lee, *Prog. Part. Nucl. Phys.* **38**, 65 (1997), 4π High Resolution Gamma Ray Spectroscopy and Nuclear Structure.
8. W. Urban, *et al.*, *Z. Phys. A* **358**, 145 (1997).
9. W. Korten and S. Lunardi, *Achievements with the Euroball spectrometer (1997-2003)* (2003).
10. M. Jentschel, *et al.*, *J. Instrum.* **12**, P11003 (2017).
11. M. Lebois, *et al.*, *Nucl. Instrum. Methods Phys. Res. A* **960**, 163580 (2020).
12. Y. Kim, *et al.*, *Eur. Phys. J. A* **53**, 162 (2017).
13. S. Biswas, *et al.*, *Phys. Rev. C* **99**, 064302 (2019).
14. S. Biswas, *et al.*, *Phys. Rev. C* **102**, 014326 (2020).
15. R. Banik, *et al.*, *Phys. Rev. C* **102**, 044329 (2020).
16. J. Dudouet, *et al.*, *Phys. Rev. Lett.* **118**, 162501 (2017).
17. J. Dudouet, *et al.*, *Phys. Rev. C* **100**, 011301 (2019).
18. K. Rezyunkina, *et al.*, *Phys. Rev. C* **106**, 014320 (2022).
19. C. Delafosse, *et al.*, *Phys. Rev. Lett.* **121**, 192502 (2018).
20. C. Delafosse *et al.*, *Acta Phys. Pol. B* **50**, 633 (2019).
21. S. Ansari, *Shape evolution in neutron-rich Zr, Mo and Ru isotopes around mass A=100*, *Theses*, Université Paris Saclay (COMUE) (2019).
22. M. Rejmund, *et al.*, *Nucl. Instrum. Methods Phys. Res. A* **646**, 184 (2011).
23. G. Montagnoli, *et al.*, *Nucl. Instrum. Methods Phys. Res. A* **547**, 455 (2005).
24. M. Rejmund, *et al.*, *Phys. Lett. B* **753**, 86 (2016).
25. M. Rejmund, *et al.*, *Phys. Rev. C* **93**, 024312 (2016).
26. J. Simpson, *et al.*, *Acta Phys. Hung. NS-H* **11**, 159 (2000).
27. Y. Kim, *et al.*, *Phys. Lett. B* **772**, 403 (2017).
28. A. Navin, *et al.*, *Phys. Lett. B* **767**, 480 (2017).
29. E. H. Wang, *et al.*, *Phys. Rev. C* **103**, 034301 (2021).
30. E. H. Wang, *et al.*, *Phys. Rev. C* **92**, 034317 (2015).
31. S. Bhattacharyya, *et al.*, *Phys. Rev. C* **98**, 044316 (2018).
32. A. Dewald, O. Möller, and P. Petkov, *Prog. Part. Nucl. Phys.* **67**, 786 (2012).
33. P. Singh, *et al.*, *Phys. Rev. Lett.* **121**, 192501 (2018).
34. T. W. Hagen, *et al.*, *Phys. Rev. C* **95**, 034302 (2017).
35. T. W. Hagen, *et al.*, *Eur. Phys. J. A* **54**, 50 (2018).
36. S. Akkoyun *et al.*, *Nucl. Instrum. Methods Phys. Res. A* **668**, 26 (2012).
37. S. Paschalis, *et al.*, *Nucl. Instrum. Methods Phys. Res. A* **709**, 44 (2013).
38. C. Stahl, *et al.*, *Comp. Phys. Comm.* **214**, 174 (2017).
39. E. Clément, *et al.*, *Nucl. Instrum. Methods Phys. Res. A* **855**, 1 (2017).
40. M. Vandebrouck, *et al.*, *Nucl. Instrum. Methods Phys. Res. A* **812**, 112 (2016).
41. J. Ljungvall, *et al.*, *Nucl. Instrum. Methods Phys. Res. A* **955**, 163297 (2020).
42. F. Recchia, *In-beam test and imaging capabilities of the AGATA prototype detector*, *Ph.D. thesis*, Università Degli Studi Di Padova (2008).
43. F. Recchia, *et al.*, *Nucl. Instrum. Methods Phys. Res. A* **604**, 555 (2009).
44. P.-A. Söderström, *et al.*, *Nucl. Instrum. Methods Phys. Res. A* **638**, 96 (2011).
45. S. Bhattacharyya, *et al.*, *Phys. Rev. Lett.* **101**, 032501 (2008).
46. M. Albers, *et al.*, *Phys. Rev. Lett.* **108**, 062701 (2012).
47. R. Casten, *Nuclear Structure from a Simple Perspective* (Oxford Science Publication, New York, 1990).
48. F. Flavigny, *et al.*, *Phys. Rev. Lett.* **118**, 242501 (2017).
49. R.-B. Gerst, *et al.*, *Phys. Rev. C* **105**, 024302 (2022).
50. F. Nowacki, *et al.*, *Phys. Rev. Lett.* **117**, 272501 (2016).
51. S. Basu and E. M. Cutchan, *Nucl. Data Sheets* **165**, 1 (2020).
52. B. Elman, *et al.*, *Phys. Rev. C* **96**, 044332 (2017).

53. K. Sieja, *et al.*, [Phys. Rev. C **88**, 034327 \(2013\)](#).
54. J. Litzinger, *et al.*, [Phys. Rev. C **92**, 064322 \(2015\)](#).
55. A. Wolf and E. Cheifetz, [Phys. Rev. Lett. **36**, 1072 \(1976\)](#).
56. B. Fogelberg, *et al.*, [Nucl. Phys. A **451**, 104 \(1986\)](#).
57. A. Astier, *et al.*, [Phys. Rev. C **85**, 054316 \(2012\)](#).
58. J. McDonald and A. Kerek, [Nucl. Phys. A **206**, 417 \(1973\)](#).
59. R. O. Hughes, *et al.*, [Phys. Rev. C **71**, 044311 \(2005\)](#).
60. O. Roberts, *et al.*, [Acta Phys. Pol. B **44**, 403 \(2013\)](#).
61. J. Genevey, *et al.*, [Phys. Rev. C **63**, 054315 \(2001\)](#).
62. S. Biswas, *et al.*, [Phys. Rev. C **93**, 034324 \(2016\)](#).